Confinement in (1+1)-dimensional $\mathbb{Z}_2$ lattice gauge theories at finite temperature

Matjaž Kebrič,[*] Jad C. Halimeh,[†] Ulrich Schollwöck, and Fabian Grusdt[‡]
Department of Physics and Arnold Sommerfeld Center for Theoretical Physics (ASC), Ludwig-Maximilians-Universität München, Theresienstraße 37, D-80333 München, Germany and Munich Center for Quantum Science and Technology (MCQST), Schellingstraße 4, D-80799 München, Germany

(Received 6 September 2023; revised 15 April 2024; accepted 3 May 2024; published 6 June 2024)

Confinement is a paradigmatic phenomenon of gauge theories, and its understanding lies at the forefront of high-energy physics. Here, we study confinement in a simple one-dimensional $\mathbb{Z}_2$ lattice gauge theory at finite temperature and filling, which is within the reach of current cold-atom and superconducting-qubit platforms. By employing matrix product states (MPS) calculations, we investigate the decay of the finite-temperature Green's function and uncover a smooth crossover between the confined and deconfined regimes. Furthermore, using the Friedel oscillations and string length distributions obtained from snapshots sampled from MPS, both of which are experimentally readily available, we verify that confined mesons remain well-defined at arbitrary finite temperature. This phenomenology is further supported by probing quench dynamics of mesons with exact diagonalization. Our results shed new light on confinement at finite temperature from an experimentally relevant standpoint.

DOI: 10.1103/PhysRevB.109.245110

I. INTRODUCTION

Lattice gauge theories (LGTs) were first proposed to unravel the intricate mechanism of quark confinement [1], which is one of the key steps towards understanding the formation of hadrons at finite temperature and their transition to quark-gluon plasma [2]. Although LGTs are still mainly considered when tackling problems in high energy physics, they are also extremely powerful when applied to condensed-matter physics [3–5]. There, confined phases emerge in many models that are used to describe strongly correlated systems [6,7], and $\mathbb{Z}_2$ LGTs have direct connections to high-T_c superconductivity [8,9]. LGTs' full power is unveiled when gauge fields are coupled to dynamical matter at finite doping, where the confinement-deconfinement transition still lacks a comprehensive theoretical description. This is also partially due to the fact that numerical simulations of LGTs are demanding [10], especially when the dimension surpasses the simplest case of one spatial and time dimension ($1+1$D) [11]. The study of LGTs becomes even more involved at finite temperature, where the usual numerical limitations are amplified.

Significant advances in quantum simulations using cold atoms in recent years introduced a new platform to study strongly correlated many-body problems [12–14]. Considerable progress has been made specifically towards quantum simulation of LGTs using cold atoms [15]. A first proof of concept of experimentally simulating a $\mathbb{Z}_2$ LGT has already been made [16,17] by employing a Floquet scheme [18]. Recently, new proposals have been put forward that utilize Rydberg tweezer arrays [19], where the tedious implementation of the gauge protection has been greatly simplified by making use of the so-called local pseudogenerators [20,21]. Furthermore, proposals using superconducting qubits have also appeared [22]. A lot of effort has also been made in using digital quantum computers [23–27] with a version of a LGT already experimentally realized [28], however limited in size.

Here we study finite-temperature properties of a simple $1+1$D $\mathbb{Z}_2$ LGT where dynamical charges are coupled to a gauge field at finite doping. This $\mathbb{Z}_2$ LGT is the simplest nontrivial LGT which can be obtained after discretization of the $U(1)$ Schwinger model to a $\mathbb{Z}_n$ LGT [29], and it is already within the reach of existing quantum simulators [15–18]. The dynamics of the gauge field is induced by an electric-field term, which also acts as a linear confining potential in the sector without background charges. As a result, individual particles become confined into mesons, which themselves remain dynamical. So far, the study of confinement in a $\mathbb{Z}_2$ LGT at finite temperature has been limited to challenging Monte Carlo calculations [30], and the sign problem could be mitigated in a $U(1)$ Schwinger model [31–33]. A theoretical study of a phase diagram at finite temperature and chemical potential utilizing digital quantum simulator algorithms has also been performed, however the study of confinement was hindered by the small system size [26].

In this work, we employ large-scale state-of-the-art matrix product states (MPS) calculations [34], where we make use of the concept of quantum purification [35–37] in order to obtain finite-temperature states. We study the decay of the $\mathbb{Z}_2$-invariant Green's function at finite temperature, which is a direct probe of confinement, and we uncover a smooth confinement-deconfinement crossover at finite temperature. This goes against the conventional wisdom where one would expect a deconfined phase at any finite temperature $T > 0$,

[*]matjaz.kebric@physik.uni-muenchen.de
[†]jad.halimeh@physik.lmu.de
[‡]fabian.grusdt@physik.uni-muenchen.de

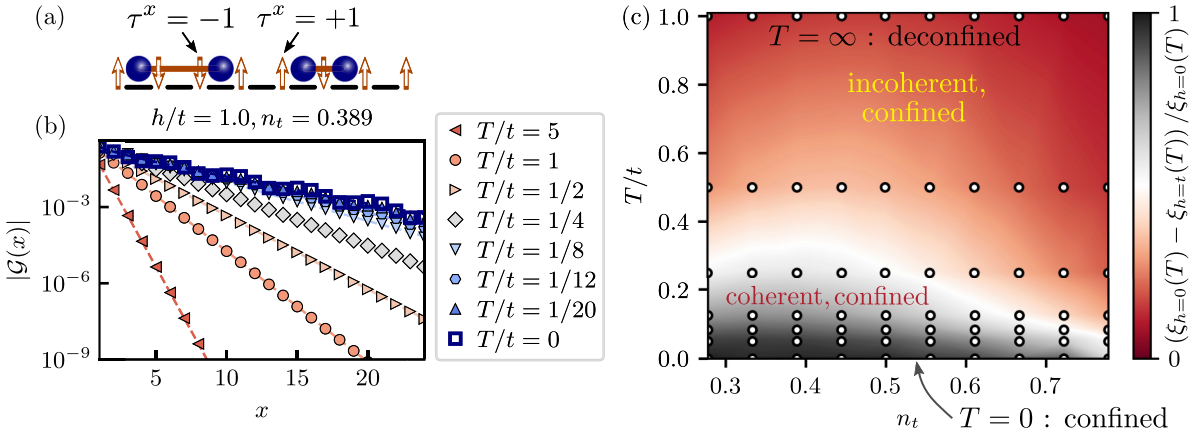

FIG. 1. (a) In the physical sector without background charges, pairs of hard-core bosons (blue spheres) are connected with the $\mathbb{Z}_2$ strings (red horizontal lines), which denote the orientation of the $\mathbb{Z}_2$ electric field. (b) Green's function (3) for different temperatures T at a constant chemical potential yielding a filling of $n_t = 0.389$ in the ground state, together with the fitting function containing exponential and power-law decay (dashed lines) [38]. (c) Heat diagram of the difference between the correlation lengths at $h = 0$ and $h = t$ as a function of target lattice filling n_t and temperature T (white dots indicate data points). For the details on exact fillings at finite temperatures, see Supplemental Material [38].

since the system has to be deconfined in the limit $T \to \infty$. In addition to the Green's function, we study Friedel oscillations, which also contain direct signatures of confinement. Furthermore, we sample snapshots from MPS and study string and antistring length histograms, which we propose as a new simple but robust measure of confinement suitable for cold-atom experiments. All these quantities, as well as dynamical quenches at finite and zero temperature, show signatures of confinement at any temperature $T < \infty$, albeit becoming less pronounced as T increases.

II. MODEL

We consider a $1+1$D $\mathbb{Z}_2$ LGT where hard-core bosons (partons) are minimally coupled to a $\mathbb{Z}_2$ gauge field [39–42],

$$\hat{\mathcal{H}} = -t \sum_j \left(\hat{a}_j^\dagger \hat{\tau}_{j,j+1}^z \hat{a}_{j+1} + \text{H.c.}\right) - h \sum_j \hat{\tau}_{j,j+1}^x. \quad (1)$$

Here $\hat{a}_j^\dagger$ ($\hat{a}_j$) are hard-core boson creation (annihilation) operators, and we represent the $\mathbb{Z}_2$ gauge and electric fields on the links between lattice sites with Pauli matrices $\hat{\tau}_{j,j+1}^z$ and $\hat{\tau}_{j,j+1}^x$. We note that in $1+1$D one can map the bosons to fermions via the Jordan-Wigner transformation [43], meaning that our results can also be extended to spinless fermions.

In addition, we consider the set of local operators [39]

$$\hat{G}_j = \hat{\tau}_{j-1,j}^x \hat{\tau}_{j,j+1}^x (-1)^{\hat{n}_j}, \quad (2)$$

where $\hat{n}_j = \hat{a}_j^\dagger \hat{a}_j$. These local operators generate the local symmetry of the $\mathbb{Z}_2$ gauge group and are the $\mathbb{Z}_2$ LGT counterpart of the Gauss law. They commute with the Hamiltonian, $[\hat{\mathcal{H}}, \hat{G}_j] = 0, \forall j$, and with each other, $[\hat{G}_j, \hat{G}_i] = 0$. The eigenvalues of $\hat{G}_j$ are $g_j = \pm 1$. The Hilbert space can thus be divided into different sectors specified by the values of g_j on each lattice site. In this work, we choose the so-called physical sector without background charges where $g_j = 1, \forall j$ [39]. Hence, the orientation of the $\mathbb{Z}_2$ electric field changes only across an occupied lattice site and it is thus convenient to define the $\mathbb{Z}_2$ electric *string* and *antistring*, which graphically represent the orientation of the electric field as $\tau^x = \mp 1$, respectively; see Fig. 1(a). We note that we do not include a staggered mass term in our LGT, which would give the vacuum state as the ground state in the Schwinger model [1,29]. This is because we are interested in finite fillings, which translates to finite hole doping in a $t - J_z$ model to which the above LGT can be exactly mapped [41].

The first term in Hamiltonian (1) is the hopping term, where the $\hat{\tau}^z$ operator ensures that the Gauss law remains satisfied, i.e., that the partons remain attached to a string. The second term induces a linear confining potential among partons connected with the same string, since strings become energetically unfavorable. In the ground state, partons connected with the same string thus become confined into mesons (dimers), where the string length is minimized. This happens for any nonzero value of $h > 0$ [40]; at $h = 0$ partons are free/deconfined [39]. A solution of the confinement problem in the ground state of this $\mathbb{Z}_2$ LGT has been found by performing a nonlocal transformation to the so-called string-length basis [41]. There, confinement can formally be understood as translational-symmetry breaking in the new basis [41].

We use the concept of quantum purification [35–37,44] in order to obtain finite-temperature states. We add an auxiliary lattice site to every physical lattice site. These are entangled to the physical lattice sites and act as a thermal bath [35]. By using DMRG [34,45], we first compute the maximally entangled state between the auxiliary and physical sites on which we then perform imaginary time evolution [46] in order to obtain states at finite temperature T [35–37]. We use SyTen [47,48], an MPS toolkit where DMRG as well as standard time evolution algorithms for MPS are implemented. For more details on the numerical calculations, see Supplemental Material [38].

For practical purposes, we consider an even number of hard-core bosons in the lattice. Since we employ open boundary conditions, we consider that the chain always starts with an antistring, i.e., a link with positive orientation $\tau_{0,1}^x = +1$ in

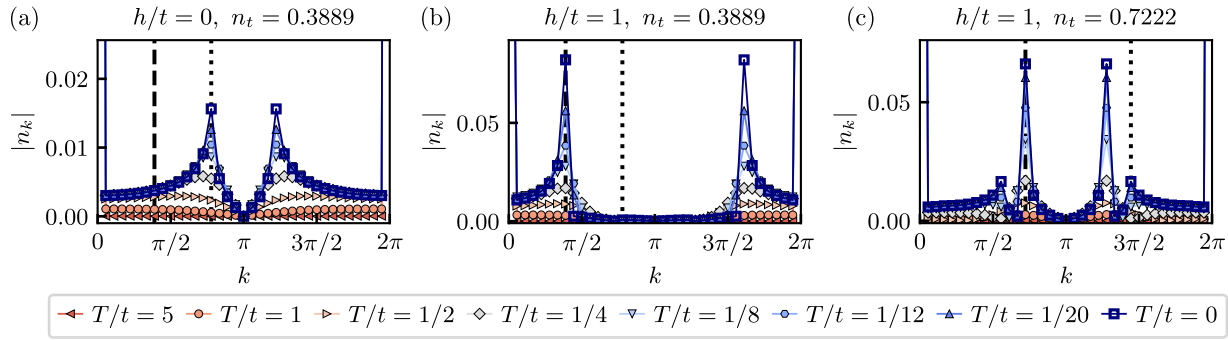

FIG. 2. Fourier transformation of Friedel oscillations. (a) Fourier coefficients $|n_k|$ in the deconfined phase exhibit broad peaks at $k = 2\pi n_t$ (vertical dotted line), which correspond to Friedel oscillations of free partons. (b) In the confined phase, the Fourier transformation exhibits peaks at $k = \pi n_t$ (vertical dashed line), which correspond to Friedel oscillations of mesons. (c) Substantial peaks are visible at $k = \pi n_t$ (vertical dashed line) and at $k = 2\pi n_t$ (vertical dotted line) at higher target filling $n_t = 26/36$ in the confined phase $h/t = 1$. Both peaks rise simultaneously with decreasing temperature T. For precise fillings at finite temperature, see Supplemental Material [38].

the confined phase when $h/t > 0$. These conditions prevent the partons from being confined to the boundaries. This is automatically satisfied in the numerical implementation with DMRG in the ground state, where we map the model to a spin-1/2 system and also add a chemical potential term proportional to μ [38].

III. GREEN'S FUNCTION

To probe the confinement of partons into mesons, we consider the $\mathbb{Z}_2$-invariant Green's function defined as [40–42]

$$\mathcal{G}(i-j) = \left\langle \hat{a}_i^\dagger \left(\prod_{i \leqslant \ell < j} \hat{\tau}^z_{\ell,\ell+1} \right) \hat{a}_j \right\rangle, \tag{3}$$

which can also be considered as a one-dimensional version of the Fredenhagen-Marcu order parameter [49]. At $T = 0$, it decays exponentially in the confined regime and with a power-law in the deconfined regime [40].

The Green's function decays exponentially in both regimes at $T > 0$, albeit with different decay rates. This makes a clear distinction between the confined and deconfined phases at finite temperature difficult. To overcome this complication, we compare the rate of decay of the Green's function (3) in both regimes and determine the crossover temperature, at which the thermal fluctuations start to dominate.

To this end, we fit the Green's function results with a function containing algebraic and exponential ($\sim e^{-|i-j|/\xi}$) decay profiles, and we extract the correlation length ξ; see Fig. 1(b) (for details, see also [38]). We consider the difference between the correlation lengths, $\Delta\xi(T) = [\xi_{h=0}(T) - \xi_{h=t}(T)]$, in the two regimes at the same temperature T and comparable target fillings n_t, for which we know that the charges are confined and deconfined in the ground state; see Fig. 1(c). From this we determine the crossover region where thermal fluctuations begin to dominate the exponential decay of the Green's function. We define the approximate crossover boundary in the region where $\xi_{h=0}(T) - \xi_{h=t}(T) = \frac{1}{2}\xi_{h=0}(T)$.

We find that the typical crossover region is at $T/t \approx 0.25$, which is also influenced by the lattice filling; see Fig. 1(c). The so-called target filling n_t is the filling obtained in the ground state at a given chemical potential μ, which is kept constant during the imaginary time evolution. The actual densities $n(T)$ at finite temperature thus deviate slightly from n_t for each run at $h/t = 0$ and $h/t = 1$, respectively. These deviations do not exceed $|n_{h=t}(T) - n_{h=0}(T)|/n(T) < 20\%$ for $T/t < 1$. We thus plot the data points as a function of n_t [38].

IV. FRIEDEL OSCILLATIONS

Another hallmark of confinement in the $1+1$D $\mathbb{Z}_2$ LGT is an abrupt change of the frequency of the Friedel oscillations in the confined phase. The frequency in the confined phase equals $2k_F = \pi n$, which is half the frequency found in the deconfined phase of free partons [40]. This indicates that the confined mesons are indeed well-defined constituents that remain mobile and form a Luttinger liquid with intricate interactions.

To analyze the Friedel oscillations at finite temperature, we perform the Fourier transformation of the density profile $\langle \hat{n}_j \rangle$ and extract the frequency of oscillations. In the deconfined phase $h/t = 0$, we observe broad peaks at $k = 2\pi n$, which is the expected frequency for the Friedel oscillations of free partons; see Fig. 2(a). The peaks are broad and only become well defined for temperatures $T/t \leqslant 1/4$. With lower temperature the peaks rise and converge to the ground-state results. Contrarily, we observe peaks at $k = \pi n$ for low temperatures in the confined phase $h/t = 1$ as expected; see Fig. 2(b). These peaks appear again at around $T/t \leqslant 1/4$ and converge to the ground-state results at lower temperature in a similar fashion to the deconfined case.

There are no deconfined peaks visible in our results for the filling of $n_t = 0.3889$ and $h/t = 1$ at any temperature, which rules out a deconfined parton gas in this regime. If the latter would exist, we would expect a shift in the peak position from $k = \pi n$ to $k = 2\pi n$ with increasing temperature. The absence of this shift thus suggests that mesons are pre-formed already well above the crossover temperature, i.e., partons are confined up to high temperatures where thermal fluctuations completely dominate the behavior of the system.

At higher fillings, $n \gtrsim 0.5$, we observe the coexistence of peaks at $k = \pi n$ and $2\pi n$; see Fig. 2(c). However, peaks

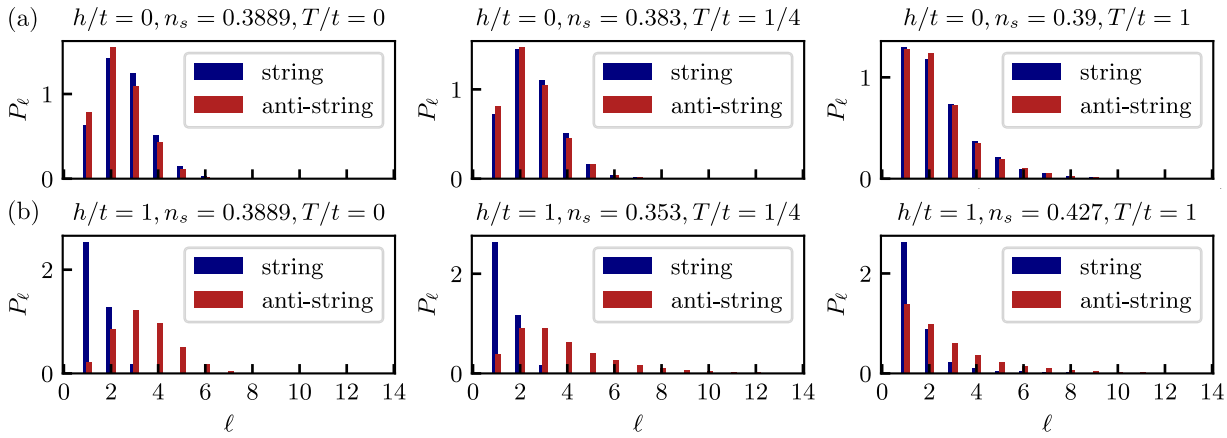

FIG. 3. String and antistring length distributions. (a) Distributions are qualitatively similar in the deconfined phase, $h = 0$, at a fixed temperature T and filling obtained from the snapshots n_s. The peaks shift to $\ell = 1$ with increasing temperature. (b) Different distributions of strings and antistrings can be observed in the confined phase $h/t = 1$. There is a strong peak at $\ell = 1$ in the string length distribution, and there are no strings with lengths larger than $\ell \geqslant 3$. In contrast, the antistring length distribution is wide, spreading over $\ell > 8$ at finite temperatures and peaking at around $\ell \approx 3$ in the ground state.

at both positions rise simultaneously with lower temperature and there is again no exchange of the position of the peaks with temperature. The peaks observed at higher fillings at $k = 2\pi n$ can be associated with hole fluctuations, which become significantly more mobile relative to mesons.

V. STRING-LENGTH DISTRIBUTIONS

Our model is within reach of modern cold-atom experiments. However, extracting the Green's function would be a rather complicated task. We therefore consider string and antistring length histograms, which are easily accessible from on-site density-resolved snapshots that can be obtained experimentally. There, one simply has to extract the number of empty lattice sites between odd-even and even-odd particles, respectively; see Supplemental Material [38] for more details. This is a robust, experimentally feasible probe of confinement, since strings are on average shorter than antistrings in the confined regime; we thus expect different distributions of strings and antistrings as a clear indicator of confinement.

To demonstrate the effectiveness of such a probe, we sample snapshots from MPS [50] using perfect sampling [51] implemented within SyTen [47,48]. The results presented in Fig. 3 show a clear difference in distributions in the confined and deconfined regimes. In the deconfined regime there is no difference between the string and antistring length distributions since partons are free; see Fig. 3(a).

In the confined phase, the string length distribution is peaked at $\ell = 1$, meaning that most of the mesonic states are tightly confined with few empty lattice sites between the two partons making up a meson; see Fig. 3(b). (There is a small fraction of mesons with $\ell \geqslant 2$, which can be attributed to quantum fluctuations. The presence of $\ell = 2$ states is in fact necessary for the mesonic states to remain mobile, since the hopping of mesons can be understood as a second-order perturbation process when we consider the limit of $h \gg t$ [40].) In contrast, the anti-string-length distribution is broad, with a long tail. Furthermore, the anti-string-length distribution has a peak at $\ell > 1$ in the ground state. This is also influenced by the overall filling of the chain; see Supplemental Material [38].

The combined bimodal distribution of string and antistring lengths is thus a clear indicator of confinement. These features are present up to temperatures consistent with our previous calculations of the Green's function and Friedel oscillations. For higher temperatures $T \geqslant t$, the distributions become more similar to each other and both peak at $\ell = 1$: this is consistent with a continuous crossover to the deconfined regime at $T = \infty$. However, at finite temperature $T \gtrsim t$, a slight difference between string and antistring length histograms remains, supporting our claim of preformed mesons up to any finite temperature.

VI. QUENCH DYNAMICS

Next we consider another experimentally accessible, dynamical probe. To this end, an initially tightly bound parton pair is introduced into a finite-density thermal gas and we probe whether it remains confined during the subsequent time evolution.

Specifically, we localize a meson on the central two sites of an L-site chain; the left (right) remaining $(L-2)/2$ sites are prepared independently in a thermal state of $\hat{\mathcal{H}}$ in Eq. (1) at a given temperature T and density $n = (N-2)/(L-2)$; see the inset in Fig. 4(a). Then, we calculate the time evolution of this initial density under the full system Hamiltonian (1), including all L sites.

We perform numerical exact simulations for $L = 12$, $N = 6$ at different values of h and T. Our results indicate no confinement at any temperature when $h = 0$, while again we find evidence of confinement at any temperature $T < \infty$ when $h > 0$: We consider dynamics of the probabilities $p_{a,b}(r)$ that the ath and bth particle, counted from the left, are r sites apart, shown in Figs. 4(a) and 4(b) for $h/t = 0$ and 1, respectively, at $T/t = 0.5$. By construction, the probability of the middle pair to be a site apart is $p_{3,4}(1) = 1$ before the quench. In the wake

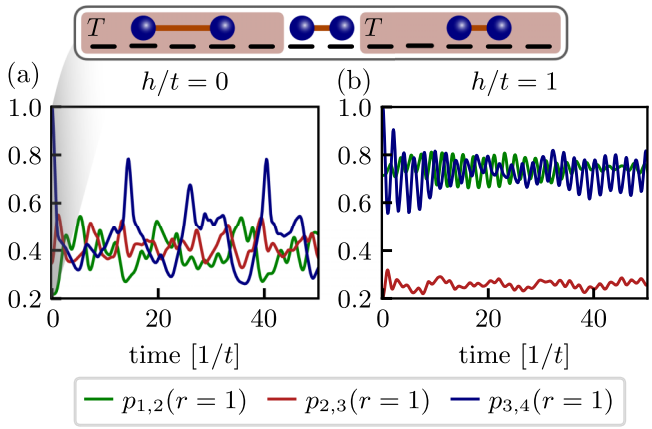

FIG. 4. Starting in a thermal ensemble at temperature $T/t = 0.5$ and at half-filling at a given value h, with a well-defined particle pair at the middle (see the inset), we quench with $\hat{\mathcal{H}}$ and calculate in ED the probabilities of a pair of particles being one site apart over evolution time. (a) In the case of $h = 0$, we find that any two consecutive pairs are equally likely to be a site apart at long evolution times. (b) When $h/t = 1$, we find that the middle pair is bound, as are the two other pairs on either side, which is indicative of confinement.

of the quench, we find a fundamental difference between zero and nonzero h. At long times, we find that when $h = 0$ any two consecutive particles are equally probable to be a site apart. On the other hand, when $h/t = 1$, we find that it is always more probable that the middle pair is bound, as well as the two pairs to its left and right, indicating confinement. This qualitative picture holds also at other values of T [38,52], but consistent with a deconfinement crossover, the signal becomes less pronounced for higher temperatures $T \to \infty$.

VII. SUMMARY AND OUTLOOK

In this work, we studied confinement in a $1+1$D $\mathbb{Z}_2$ LGT at finite temperature. We considered a $\mathbb{Z}_2$-invariant Green's function as the direct probe of confinement at finite temperature, where we uncovered a smooth confinement-deconfinement crossover at approximately $T/t \approx 0.25$. By additionally considering the Friedel oscillations, where the confinement manifests itself in halving of the frequency, we confirmed that the confinement-deconfinement crossover extends up to temperatures where the thermal fluctuations dominate the behavior of the system. These results were furthermore affirmed by the string and antistring length distributions that we proposed as an experimentally feasible, robust measure of confinement. Finally, we complemented our results with dynamical probes, also experimentally readily accessible in current state-of-the-art quantum simulators [53]. There, we showed that, again, confinement persists up to high temperatures, albeit signatures of confinement become less pronounced as the system approaches the deconfined infinite-temperature state.

Our results pave the way towards understanding confinement crossover at finite temperature in a simple $1+1$D $\mathbb{Z}_2$ LGT with dynamical matter, which can be probed with current quantum simulators. We show that the partons remain confined at low temperature, with a smooth crossover at finite temperature to an incoherent regime dominated by thermal fluctuations. At any finite temperature $T < \infty$, signatures of confinement remain. This result challenges the conventional reasoning in one dimension, where one would naively expect a deconfined regime at any finite temperature as the system is deconfined for $T \to \infty$. We expect that our results can be extended to higher gauge groups and models with more complicated interactions. Our work paves the way for explorations of confinement in state-of-the-art analog, or digital, quantum simulators, which naturally include thermal fluctuations. Such setups can also naturally explore mixed-dimensional settings of coupled 1D chains, where even richer confinement-deconfinement physics can be expected [30].

ACKNOWLEDGMENTS

We thank Annabelle Bohrdt, Zohreh Davoudi, Lukas Homeier, Mattia Moroder, Henning Schlömer, Alexander Schuckert, and Christopher White for fruitful discussions. This research was funded by the Deutsche Forschungsgemeinschaft (DFG, German Research Foundation) under Germany's Excellence Strategy – EXC-2111 – 390814868 and via Research Unit FOR 2414 under Project No. 277974659, and received funding from the European Research Council (ERC) under the European Union's Horizon 2020 research and innovation programme (Grant Agreement No. 948141) — ERC Starting Grant SimUcQuam. J.C.H. and F.G. acknowledge funding within the QuantERA II Programme that has received funding from the European Union's Horizon 2020 research and innovation programme under Grand Agreement No. 101017733, support by the QuantERA grant DYNAMITE, and by the Deutsche Forschungsgemeinschaft (DFG, German Research Foundation) under Project No. 499183856.

[1] K. G. Wilson, Confinement of quarks, Phys. Rev. D **10**, 2445 (1974).
[2] J. I. Kapusta and C. Gale, *Finite-Temperature Field Theory* (Cambridge University Press, Cambridge, UK, 2006).
[3] F. J. Wegner, Duality in generalized Ising models and phase transitions without local order parameters, J. Math. Phys. **12**, 2259 (1971).
[4] J. B. Kogut, An introduction to lattice gauge theory and spin systems, Rev. Mod. Phys. **51**, 659 (1979).
[5] X.-G. Wen, *Quantum Field Theory of Many-Body Systems* (Oxford University Press, New York, 2004).
[6] R. D. Sedgewick, D. J. Scalapino, and R. L. Sugar, Fractionalized phase in an XY$-Z_2$ gauge model, Phys. Rev. B **65**, 054508 (2002).
[7] S. Sachdev and D. Chowdhury, The novel metallic states of the cuprates: Topological Fermi liquids and strange metals, Prog. Theor. Exp. Phys. **2016**, 12C102 (2016).

[8] P. A. Lee, From high temperature superconductivity to quantum spin liquid: Progress in strong correlation physics, Rep. Prog. Phys. **71**, 012501 (2008).

[9] T. Senthil and M. P. A. Fisher, Z_2 gauge theory of electron fractionalization in strongly correlated systems, Phys. Rev. B **62**, 7850 (2000).

[10] M. C. Bañuls, K. Cichy, J. I. Cirac, K. Jansen, and S. Kühn, Density induced phase transitions in the Schwinger model: A study with matrix product states, Phys. Rev. Lett. **118**, 071601 (2017).

[11] G. Magnifico, T. Felser, P. Silvi, and S. Montangero, Lattice quantum electrodynamics in (3+1)-dimensions at finite density with tensor networks, Nat. Commun. **12**, 3600 (2021).

[12] M. Greiner, O. Mandel, T. Esslinger, T. W. Hänsch, and I. Bloch, Quantum phase transition from a superfluid to a Mott insulator in a gas of ultracold atoms, Nature (London) **415**, 39 (2002).

[13] I. Bloch, J. Dalibard, and W. Zwerger, Many-body physics with ultracold gases, Rev. Mod. Phys. **80**, 885 (2008).

[14] I. Bloch, J. Dalibard, and S. Nascimbène, Quantum simulations with ultracold quantum gases, Nat. Phys. **8**, 267 (2012).

[15] M. Aidelsburger, L. Barbiero, A. Bermudez, T. Chanda, A. Dauphin, D. González-Cuadra, P. R. Grzybowski, S. Hands, F. Jendrzejewski, J. Jünemann, G. Juzeliūnas, V. Kasper, A. Piga, S.-J. Ran, M. Rizzi, G. Sierra, L. Tagliacozzo, E. Tirrito, T. V. Zache, J. Zakrzewski *et al.*, Cold atoms meet lattice gauge theory, Philos. Trans. R. Soc. A **380** (2021),.

[16] C. Schweizer, F. Grusdt, M. Berngruber, L. Barbiero, E. Demler, N. Goldman, I. Bloch, and M. Aidelsburger, Floquet approach to $\mathbb{Z}_2$ lattice gauge theories with ultracold atoms in optical lattices, Nat. Phys. **15**, 1168 (2019).

[17] F. Görg, K. Sandholzer, J. Minguzzi, R. Desbuquois, M. Messer, and T. Esslinger, Realization of density-dependent peierls phases to engineer quantized gauge fields coupled to ultracold matter, Nat. Phys. **15**, 1161 (2019).

[18] L. Barbiero, C. Schweizer, M. Aidelsburger, E. Demler, N. Goldman, and F. Grusdt, Coupling ultracold matter to dynamical gauge fields in optical lattices: From flux attachment to $\mathbb{Z}_2$ lattice gauge theories, Sci. Adv. **5**, eaav7444 (2019).

[19] L. Homeier, A. Bohrdt, S. Linsel, E. Demler, J. C. Halimeh, and F. Grusdt, Realistic scheme for quantum simulation of $\mathbb{Z}_2$ lattice gauge theories with dynamical matter in (2+1)D, Commun. Phys. **6**, 127 (2023).

[20] J. C. Halimeh, L. Homeier, H. Zhao, A. Bohrdt, F. Grusdt, P. Hauke, and J. Knolle, Enhancing disorder-free localization through dynamically emergent local symmetries, PRX Quantum **3**, 020345 (2022).

[21] J. C. Halimeh, L. Homeier, C. Schweizer, M. Aidelsburger, P. Hauke, and F. Grusdt, Stabilizing lattice gauge theories through simplified local pseudogenerators, Phys. Rev. Res. **4**, 033120 (2022).

[22] L. Homeier, C. Schweizer, M. Aidelsburger, A. Fedorov, and F. Grusdt, $\mathbb{Z}_2$ lattice gauge theories and Kitaev's toric code: A scheme for analog quantum simulation, Phys. Rev. B **104**, 085138 (2021).

[23] E. Zohar, A. Farace, B. Reznik, and J. I. Cirac, Digital quantum simulation of $\mathbb{Z}_2$ lattice gauge theories with dynamical fermionic matter, Phys. Rev. Lett. **118**, 070501 (2017).

[24] R. Irmejs, M. C. Banuls, and J. I. Cirac, Quantum simulation of $\mathbb{Z}_2$ lattice gauge theory with minimal requirements, Phys. Rev. D **108**, 074503 (2023).

[25] G. Pardo, T. Greenberg, A. Fortinsky, N. Katz, and E. Zohar, Resource-efficient quantum simulation of lattice gauge theories in arbitrary dimensions: Solving for Gauss's law and fermion elimination, Phys. Rev. Res. **5**, 023077 (2023).

[26] Z. Davoudi, N. Mueller, and C. Powers, Toward quantum computing phase diagrams of gauge theories with thermal pure quantum states, Phys. Rev. Lett. **131**, 081901 (2023).

[27] M. Fromm, O. Philipsen, M. Spannowsky, and C. Winterowd, Simulating $\mathbb{Z}_2$ lattice gauge theory with the variational quantum thermalizer, EPJ Quantum Technol. **11**, 20 (2024).

[28] J. Mildenberger, W. Mruczkiewicz, J. C. Halimeh, Z. Jiang, and P. Hauke, Probing confinement in a $\mathbb{Z}_2$ lattice gauge theory on a quantum computer, arXiv:2203.08905.

[29] E. Ercolessi, P. Facchi, G. Magnifico, S. Pascazio, and F. V. Pepe, Phase transitions in Z_n gauge models: Towards quantum simulations of the Schwinger-Weyl QED, Phys. Rev. D **98**, 074503 (2018).

[30] F. Grusdt and L. Pollet, $\mathbb{Z}_2$ parton phases in the mixed-dimensional $t - J_z$ Model, Phys. Rev. Lett. **125**, 256401 (2020).

[31] C. Gattringer, T. Kloiber, and V. Sazonov, Solving the sign problems of the massless lattice Schwinger model with a dual formulation, Nucl. Phys. B **897**, 732 (2015).

[32] C. Gattringer, T. Kloiber, and M. Müller-Preussker, Dual simulation of the two-dimensional lattice U(1) gauge-Higgs model with a topological term, Phys. Rev. D **92**, 114508 (2015).

[33] C. Gattringer and K. Langfeld, Approaches to the sign problem in lattice field theory, Int. J. Mod. Phys. A **31**, 1643007 (2016).

[34] U. Schollwöck, The density-matrix renormalization group in the age of matrix product states, Ann. Phys. **326**, 96 (2011).

[35] A. E. Feiguin and S. R. White, Finite-temperature density matrix renormalization using an enlarged Hilbert space, Phys. Rev. B **72**, 220401(R) (2005).

[36] M. Zwolak and Guifré Vidal, Mixed-state dynamics in one-dimensional quantum lattice systems: A time-dependent superoperator renormalization algorithm, Phys. Rev. Lett. **93**, 207205 (2004).

[37] A. Nocera and G. Alvarez, Symmetry-conserving purification of quantum states within the density matrix renormalization group, Phys. Rev. B **93**, 045137 (2016).

[38] See Supplemental Material at http://link.aps.org/supplemental/10.1103/PhysRevB.109.245110 for details on the numerical simulations of the ground state, finite-temperature simulations, Green's function fits, Friedel oscillations, string and anti-string length distributions from snapshots, and details on dynamical calculations.

[39] C. Prosko, S.-P. Lee, and J. Maciejko, Simple Z_2 lattice gauge theories at finite fermion density, Phys. Rev. B **96**, 205104 (2017).

[40] U. Borla, R. Verresen, F. Grusdt, and S. Moroz, Confined phases of one-dimensional spinless fermions coupled to Z_2 gauge theory, Phys. Rev. Lett. **124**, 120503 (2020).

[41] M. Kebrič, L. Barbiero, C. Reinmoser, U. Schollwöck, and F. Grusdt, Confinement and Mott transitions of dynamical charges in one-dimensional lattice gauge theories, Phys. Rev. Lett. **127**, 167203 (2021).

[42] M. Kebrič, U. Borla, U. Schollwöck, S. Moroz, L. Barbiero, and F. Grusdt, Confinement induced frustration in a one-dimensional Z_2 lattice gauge theory, New J. Phys. **25**, 013035 (2023).

[43] P. Jordan and E. Wigner, Über das paulische äquivalenzverbot, Z. Phys. **47**, 631 (1928).

[44] A. E. Feiguin and I. Klich, Hermitian and non-Hermitian thermal Hamiltonians, arXiv:1308.0756.

[45] S. R. White, Density matrix formulation for quantum renormalization groups, Phys. Rev. Lett. **69**, 2863 (1992).

[46] S. Paeckel, T. Köhler, A. Swoboda, S. R. Manmana, U. Schollwöck, and C. Hubig, Time-evolution methods for matrix-product states, Ann. Phys. **411**, 167998 (2019).

[47] C. Hubig, F. Lachenmaier, N.-O. Linden, T. Reinhard, L. Stenzel, A. Swoboda, M. Grundner, and S. Mardazad, The SyTen toolkit (2023).

[48] C. Hubig, Symmetry-Protected Tensor Networks, Ph.D. thesis, LMU München, 2017.

[49] K Gregor, D. A. Huse, R Moessner, and S L Sondhi, Diagnosing deconfinement and topological order, New J. Phys. **13**, 025009 (2011).

[50] M. Buser, U. Schollwöck, and F. Grusdt, Snapshot-based characterization of particle currents and the Hall response in synthetic flux lattices, Phys. Rev. A **105**, 033303 (2022).

[51] A. J. Ferris and G. Vidal, Perfect sampling with unitary tensor networks, Phys. Rev. B **85**, 165146 (2012).

[52] Videos of time evolution of parton-separation probabilities.

[53] Y. Kuno, S. Sakane, K. Kasamatsu, I. Ichinose, and T. Matsui, Quantum simulation of (1+1)-dimensional U(1) gauge-Higgs model on a lattice by cold Bose gases, Phys. Rev. D **95**, 094507 (2017).